Original Article

Insights into corrosion behaviour of uncoated Mg alloys for biomedical applications in different aqueous media

C.S. Neves [a,*], I. Sousa [a], M.A. Freitas [a], L. Moreira [b,c,d], C. Costa [b,c,d], J.P. Teixeira [b,c,d], S. Fraga [b,c,d], E. Pinto [e,f], A. Almeida [e], N. Scharnagl [h], M.L. Zheludkevich [g,h], M.G.S. Ferreira [a], J. Tedim [a]

[a] *Department of Materials Engineering and Ceramics, CICECO, University of Aveiro, Aveiro, 3810-193, Portugal*
[b] *Departamento de Saúde Ambiental, Instituto Nacional de Saúde Doutor Ricardo Jorge, Rua Alexandre Herculano 321, Porto, 4000-055, Portugal*
[c] *EPIUnit - Instituto de Saúde Pública, Universidade do Porto, Rua das Taipas 135, Porto, 4050-600, Portugal*
[d] *Laboratório para a Investigação Integrativa e Translacional em Saúde Populacional (ITR), Rua das Taipas 135, Porto, 4050-600, Portugal*
[e] *LAQV/REQUIMTE, Departamento de Ciências Químicas, Faculdade de Farmácia, Universidade do Porto, Rua Jorge Viterbo Ferreira, 228, Porto, 4050-313, Portugal*
[f] *Departamento de Saúde Ambiental, Escola Superior de Saúde do Instituto Politécnico do Porto, R. Dr. António Bernardino de Almeida 400, Porto, 4200-072, Portugal*
[g] *Institute for Materials Science, Faculty of Engineering, University of Kiel, Kaiserstraße 2, Kiel, 24143, Germany*
[h] *Institute of Surface Science, Helmholtz-Zentrum Hereon, Max-Planck Straße 1, Geesthacht, 21502, Germany*

ARTICLE INFO

ABSTRACT

MgCa and MgGd series of alloys are often reported as promising candidates for biomedical applications. In the present study, cytotoxicity and corrosion behavior of Mg1Ca and Mg10Gd alloys in different electrolytes (NaCl, PBS, MEM) have been investigated in order to make a direct comparison and understand the mechanisms behind their performance. Potentiodynamic polarization and electrochemical impedance spectroscopy (EIS) were employed to analyze corrosion processes depending on media composition, whereas X-Ray diffraction (XRD) and scanning electron microscopy (SEM) were used to evaluate crystalline structure, phase composition and surface morphology of the corroded substrates after immersion in the different electrolytes. Moreover, cytotoxicity of the Mg alloys was assessed using the WST-1 reduction and lactate dehydrogenase (LDH) release assays in L929 mouse fibroblasts. The electrochemical results showed that Mg1Ca has a lower degradation rate when compared to Mg10Gd, due to the lower microgalvanic effects and the presence of Ca as an alloying element. Furthermore, the corrosion activity is reduced in MEM, for both alloys, when compared to NaCl and PBS. The cytotoxicity assays revealed that Mg10Gd was cytotoxic in all the conditions tested, while the toxicity of Mg1Ca was low. Overall, these findings show that Mg1Ca alloy presents a higher corrosion resistance and biocompatibility and is a promising material to be used in biomedical implants.

* Corresponding author.
 E-mail address: cristina.neves@ua.pt (C.S. Neves).

1. Introduction

Metallic materials play an important role in biomedical and tissue engineering fields due to the combination of high mechanical strength and fracture toughness, which makes them more suitable for load-bearing applications than ceramics or polymeric materials [1]. Currently, the most used metallic materials for biomedical implants are stainless steel, CoCr based alloys, and titanium based alloys [1—3]. However, the release of toxic or potentially harmful products, from these materials, through wear corrosion processes is a major concern [4]. Furthermore, these materials act as permanent implants that must be surgically removed after the tissue has healed, which increases health risks and associated costs. Biodegradable materials are a novel class of biomaterials that degrade within the body after supporting the healing process of a diseased tissue or organ. Among these, biodegradable metals such as magnesium (Mg) and its alloys have been gaining an increasing interest from a biomedical application perspective since Mg is exceptionally light in weight and exhibits good mechanical properties. In addition, Mg is biocompatible and essential to human metabolism due to magnesium's role in several metabolic processes. Nevertheless, a considerable challenge is the limited corrosion resistance of Mg and its alloys [5]. This metal readily reacts with water as its reduction potential is very negative ($E° = -2.4$ V vs. SHE). Even if such high reactivity is envisaged as a negative feature for areas where production of durable structures is required, the same does not necessarily apply to other areas. In fact, literature in the biomedical field has devoted a substantial attention to the use of Mg alloys as biodegradable biomedical implants [6,7], as it combines a set of unique properties: (i) Mg alloys biocompatibility, (ii) the physiological relevance of the Mg^{2+} ions generated and (iii) the mechanical properties, namely its elastic modulus, which matches the modulus of the bone better than other metallic alloys [8]. However, the main challenge is its uncontrolled and fast inhomogeneous degradation, with one of main consequences being evolution of H_2 [6], enclosing pernicious effects to the human body. Mg and its alloys are known to depict different forms of corrosion: galvanic corrosion, localized corrosion, stress corrosion cracking, corrosion fatigue, among others [9,10]. Furthermore, corrosion of Mg alloys depends greatly on their composition and microstructure (grain size, shape and distribution of second phases), post-processing and media. In most cases, localized corrosion, such as pitting corrosion, generally occurs due to microgalvanic corrosion between the intermetallic compounds and their neighboring α-Mg matrix [11].

Song and Atrens (1999, 2003), in their work, have suggested that the two main reasons for poor corrosion resistance of Mg and its alloys are internal galvanic corrosion (caused by second phases or impurities) and the instability of the quasi-passive hydroxide film formed at Mg surface (which leads to poor pitting resistance) [9,10].

Mg dissolution in aqueous environments usually follows an electrochemical reaction where its reaction with water leads to the production of magnesium hydroxide and hydrogen gas. Corrosion of magnesium and its alloys is mainly localized and in the form of irregular pitting (Song 2003). This is due to the fact that, in water, the magnesium hydroxide accumulated on the underlying magnesium matrix, acts as a corrosion protective layer but when the chloride concentration is high, magnesium hydroxide converts into the highly soluble magnesium chloride, leading to severe pitting corrosion [12]. In magnesium alloys, elements (impurities) and cathodic sites with low hydrogen overpotential facilitate hydrogen evolution, thus causing substantial galvanic corrosion rates and local gas cavities. However, this is a "general rule" and, it must be taken into consideration that the corrosion morphology of magnesium and its alloys depends on the alloy chemistry and environmental conditions. For Mg alloys the corrosion mechanism is more complicated than that of pure Mg [10].

The microstructure constituents of Mg alloys are usually characterized by the α-Mg matrix and second phase or intermetallic phases, such as Mg_2Ca in Ca-containing alloys. Since, in most cases, the electrode potential of these second phases is significantly higher than that of the α-Mg substrate, dissolution tends to emerge in the α-Mg matrix around second-phase particles. There are reports of the presence of small Mg_2Ca particles in coexistence with Fe and Si results in pitting corrosion of Mg—Ca alloys [12].

Nevertheless, independently of the interaction among alloying elements, the α phase matrix always corrodes preferentially (when elements and impurities are within tolerance levels), while the alloying elements act as cathodes to the α phase or as corrosion barriers more resistant than the α matrix phase [9].

In order to overcome this uncontrolled degradation several strategies have been studied, from the development of new alloys [7,13,14] to surface modification and coating technologies [7,15—18].

Before considering any modification to the Mg substrate it is relevant to investigate if a correlation between the tests performed in simplified electrolyte solutions and body fluids exists. There are groups supporting the use of more simplified electrolyte compositions, as the understanding of corrosion processes, as well as the type of inhibiting product layers formed are easier to investigate. Others support that a real development of materials requires testing under conditions close to the ones of application, though the development of more realistic factors of performance is obtained at the expense of loss of mechanistic information.

Overall, several works have shown that the level of degradation of Mg depends on the electrolyte composition

Table 1 − Summary of the main elements found in chemical composition of the Mg alloys.

	Gd %	Ca %	Fe %	Cu %	Ni %	Be %
Mg1Ca	—	1.029 ± 0.038	$4.40 \times 10^{-3} \pm 8.04 \times 10^{-4}$	$1.26 \times 10^{-3} \pm 3.20 \times 10^{-5}$	$6.16 \times 10^{-4} \pm 1.02 \times 10^{-5}$	—
Mg10Gd	8.55 ± 0.15	—	$5.06 \times 10^{-3} \pm 1.21 \times 10^{-4}$	$5.50 \times 10^{-4} \pm 1.18 \times 10^{-5}$	$1.04 \times 10^{-4} \pm 9.68 \times 10^{-6}$	$1.70 \times 10^{-6} \pm 1.070 \times 10^{-6}$

Table 2 − Composition of the different electrolytes.

NaCl	PBS (Phosphate Buffer solution)		MEM (Minimum essential medium)	
2.9 g/L	NaCl	8.0 g/L	$CaCl_2.2H_2O$	0.26 g/L
			$MgSO_4.7H_2O$	0.20 g/L
	KCl	0.2 g/L	NaCl	6.8 g/L
			KCl	0.40 g/L
	Na_2HPO_4	1.44 g/L	$NaHCO_3$	2.2 g/L
			$NaH_2PO_4.2H_2O$	0.16 g/L
			Aminoacids	
	KH_2PO_4	0.24 g/L	Vitamins	
			D-Glucose	1 g/L
			Phenol Red	

used [7,19−24]. This is not entirely surprising, as the presence of different inorganic components, amino acids, vitamins or glucose can affect the formation of the corrosion product layers and affect the degradation kinetics of the alloys. Recently, the interaction of different components of physiological solutions on the degradation of Mg and its alloys was investigated in more detail. Both works from Agha [22] and Mei [24] have shown that a synergistic effect on suppression of Mg degradation occurs when Ca^{2+}, PO_4^{3-} and HCO_3^- are simultaneously present in the solution. In particular, the work of Mei has additionally shown that the formation of a protective layer by the combining effect of Ca^{2+}, Mg^{2+}, HPO_4^{2-} and HCO_3^- is no longer observed when pH buffers with complexing ability towards Ca^{2+} and Mg^{2+} (e.g. Tris/HCl) are present in solution or when one of the three critical species is not present.

Several Mg alloys have been investigated as candidates for biomedical applications, namely as orthopedic and cardiovascular implants. Generally, Mg alloys contain aluminum (Al) or rare earth elements (REEs) [12] and there is a number of reported studies mainly focused on Mg−Al and Mg-RE alloy systems [25−28]. Results showed that both alloys achieve similar results to other biomaterials, no signs of systemic toxicity and therefore considered realistic alternatives to permanent implants. Despite the fact that biodegradable Mg alloys, containing Al or rare earth elements, exhibit good mechanical properties and better corrosion resistance, the presence of such constituents raises concerns about their safety for human health. Aluminum is a well known neurotoxicant and it has been suggested to be associated with various neurological disorders [29]. Additionally, intravenous administration of cerium, praseodymium and yttrium has also been associated with acute hepatotoxicity [30]. Consequently, in order to assure the biocompatibility of biodegradable materials, more efforts have been made to develop new types of Mg alloys, using elements with no or low toxicity as alloying elements.

In this work, we investigate two Mg alloys for biomedical application: Mg1Ca and Mg10Gd. The selection of a Mg−Ca alloy is based upon the fact that Ca encloses two main advantages when used in alloys as bioabsorbable implants: i) it is the major component in the human bone and ii) the combination of Mg^{2+} and Ca^{2+} ions can be beneficial for bone healing [31]. On the other hand, the introduction of Gd aims at

improving strength and corrosion resistance. However, the effects on human health of this rare earth element are still uncertain and a matter of concern. Regarding their degradation behavior, reports in the literature reveal that the appropriate content of Ca in Mg–Ca alloys should be in the range of 0.6–1 wt% whereas for Gd, a highly soluble element in Mg, the optimal content is 5wt% [32].

Consequently, the aim of this work is two-fold: (i) selection of an appropriate media for corrosion testing and (ii) *in vitro* cytotoxicity evaluation of both Mg alloys according to ISO 10993–5:2009 on biological evaluation of medical devices.

2. Experimental section

2.1. Materials and methods

All the chemicals were obtained from Sigma–Aldrich, with >98% of ground substance, and used as received. Cell culture medium, supplements and reagents were purchased from Gibco, Thermo Fisher Scientific, USA.

2.2. Mg alloys chemical analysis and pre-treatments

Mg10Gd and Mg1Ca cast at Helmholtz-Zentrum Greesthacht (HZG), Greeshacht, Germany, were the biodegradable Mg alloys selected for the proposed studies. Elemental analysis of the acid-digested (1:1:1 HNO_3 65% + HCl 32% + H_2O) Mg1Ca and Mg10Gd alloys and their extracts was performed by inductively coupled plasma mass spectrometry (ICP-MS) using an iCAP™ Q instrument (Thermo Fisher Scientific, Bremen, Germany). Calibration standards ranging from 1 to 1000 μg/L were prepared from three multi-element commercial standard solution: Periodic table mix 1, Periodic table mix 3 and Transition metal mix 2 (all from Sigma–Aldrich, Buchs, Switzerland). The element rhodium (Rh) was used as internal standard (IS). A IS solution was prepared at a concentration of 100 μg/L by appropriate dilution of a 1000 mg/L Rh standard solution (Sigma–Aldrich, Buchs, Switzerland). This solution was added to both samples and calibration standard solutions in order to obtain a final IS concentration of 10 μg/L. The following elemental isotopes (*m/z* ratios) were monitored: ^{7}Li, ^{9}Be, ^{26}Mg, ^{27}Al, ^{43}Ca, ^{51}V, ^{52}Cr, ^{55}Mn, ^{57}Fe, ^{59}Co, ^{60}Ni, ^{65}Cu, ^{66}Zn, ^{71}Ga, ^{75}As, ^{82}Se, ^{88}Sr, ^{89}Y, ^{90}Zr, ^{93}Nb, ^{98}Mo, ^{107}Ag, ^{111}Cd, ^{118}Sn, ^{121}Sb, ^{133}Cs, ^{137}Ba, ^{139}La, ^{140}Ce, ^{141}Pr, ^{146}Nd, ^{147}Sm, ^{153}Eu, ^{157}Gd, ^{159}Tb, ^{163}Dy, ^{165}Ho, ^{166}Er, ^{169}Tm, ^{172}Yb, ^{175}Lu, ^{178}Hf, ^{181}Ta, ^{182}W, ^{205}TI, ^{208}Pb and ^{209}Bi. Duplicates of each sample were prepared and analysed independently. The chemical composition is displayed in Table 1 and the results are presented as the calculated mean and standard error. Mg alloys were surface polished using silicon carbide (SiC) paper (from 400 to 2500 grit) and then rinsed with isopropanol and dried in a warm stream of air.

2.3. Physical measurements

Mg10Gd and Mg1Ca substrates were investigated from a corrosion standpoint using potentiodynamic polarization and electrochemical impedance spectroscopy (EIS).

Potentiodynamic polarization and EIS measurements were carried out in a three-electrode cell with a SCE reference electrode, a platinum foil counter electrode and the Mg alloy sample (Mg10Gd or Mg1Ca) as the working electrode (exposed area of ca. 2.27 cm^2). The cell was placed in a Faraday cage to avoid the interference of external electromagnetic fields. The electrolytes used consisted of 0.05 M NaCl aqueous solution, 10 mM PBS aqueous solution and MEM − minimum essential medium. The composition of the different electrolytes is shown in Table 2. The measurements were performed using a Gamry FAS2 Femtostat with PCI4 Controller. Tafel extrapolation of cathodic polarization curves (E *vs* log(i)) was used to determine the corrosion current density, i_{corr} (mA cm^{-2}). The analysis was made by selecting the linear part of the cathodic curve, with at least one decade of current density variation, that started at ≈100 mV in respect to the corrosion potential (Ecorr). The current value at the E_{corr} intersection gave the corrosion current density, i_{corr}.

Only the cathodic branches were used for semi-quantitative estimation of the corrosion current density at specific moment, since for the studied systems the anodic kinetics do not exhibit activation control and do not follow the Tafel law.

For EIS measurements, the selected frequency range was from 10^5 to 10^{-2} Hz, with a 10 mV rms of sinusoidal perturbation with 10 points per frequency decade. All the spectra were recorded at open circuit potential. For the potentiodynamic polarization curves the anodic and cathodic branches were obtained independently from the corrosion potential (±500 mV) at a potential scan rate of 1 mV/s after 1 h of immersion in the corresponding medium. All electrochemical tests were performed at atmospheric pressure and room temperature and carried out in triplicate to check the reproducibility of the results.

Weight loss measurements were performed by immersion of the alloys in MEM, PBS and 0.05 M NaCl, according to the ASTM G31-72 standard. Each Mg alloy was immersed in the respective media, in triplicate, at room temperature, using a solution volume/surface area ratio of 25 mL/cm^2. After 2 and 7 days, samples were extracted and immersed in chromic acid solution to remove corrosion products. Samples were then washed with distilled water, acetone, dried in a stream of warm hair and weighted.

Weight loss was calculated by the difference between the weight before and after the immersion divided by the sample exposed area.

The surface morphology of the samples was characterized on a Hitachi (S-4100) scanning electron microscope equipped with energy dispersive spectroscopy (SEM-EDS) operating at an acceleration voltage of 25 kV. Prior to SEM analysis, the samples were sputtered with a thin layer of conductive carbon onto their surfaces.

Samples were analyzed by X-Ray diffraction (XRD) to study the crystal structure and phase composition. XRD data were collected at room temperature using a PANalytical X'Pert MPD PRO diffractometer (Bragg–Brentano geometry, Ni-filtered Cu Kα radiation, PIXcel^{1D} detector, step 0.02°). The exposure time corresponded to about 2 s per step over the angular range of 4–80°.

2.4.   *Preparation of Mg alloys extracts for cytotoxicity testing*

Mg1Ca and Mg10Gd alloys were cut into circular disks with 1.7 cm in diameter and 0.5 cm in height. Extracts of the bare Mg1Ca and Mg10Gd disks were prepared according to ISO 10993—12:2012 [33]. Prior to extraction, the Mg alloy disks were sterilized by UV radiation for 2 h (1 h per side). The extraction was carried out in borosilicate glass containers for 24 and 72 h at 37 °C with gentle agitation (60 rpm), using MEM containing 4 mM L-glutamine, 100 units/mL of penicillin and 100 μg/mL of streptomycin as extraction medium, at a surface area-to-extractant volume ratio of 1.25 cm^2/mL. The liquid extracts were tested for cytotoxicity immediately after preparation to prevent sorption onto the extraction container or other changes in their composition.

2.5.   In vitro *cytotoxicity testing of the Mg alloys extracts*

The cytotoxic potential of the Mg alloys extracts was investigated in the mouse connective tissue L929 cell line, as recommended by ISO 10993—5:2009 [33]. L929 cells obtained from the American Type of Culture Collection (ATCC; CCL1) were maintained in a humidified atmosphere of 5% CO_2-95% air at 37 °C and cultured in MEM supplemented with 4 mM L-glutamine, 100 units/mL of penicillin, 100 μg/mL of streptomycin and 10% of heat inactivated fetal bovine serum (FBS). Cells were passaged at 80% confluence using a trypsin—EDTA 0.25% solution, seeded in flat bottom 96 well plates at a density of 10.000 cells/well and medium changed 24 h after seeding. Cells were exposed for 24 h to the direct (1x), 1:2, 1:4 and 1:8 diluted extracts at 48 h after seeding. Cells exposed to the extraction medium, diluted in the same % served as controls. Cytotoxicity of the extracts was evaluated using the WST-1 reduction and lactate dehydrogenase (LDH) release assays. Cells incubated for 30 min with 0.2% Triton X-100 and 70% ethanol served as positive controls (PC) for the LDH release and WST-1 reduction assays, respectively. For LDH release determination, the incubation medium of each well was gently transferred to a round bottom microplate at the end of the exposure period and centrifuged for 5 min at 2000×*g* to remove the cell debris. 100 μL of supernatant were gently

transferred to a clean flat bottom microplate and the assay carried out according to the manufacturer's instructions (Roche Applied Sciences, Mannheim, Germany). Absorbance was measured at 490 nm and 630 nm (reference wavelength) in a microplate reader (SpectraMax iD3, Molecular Devices, USA). Data was expressed in percentage of LDH release relative to the PC. For WST-1 reduction determination, the incubation medium was aspirated and cells incubated for 2 h, at 37 °C and 5% CO_2, with 100 μL/well of Cell Proliferation Reagent WST-1 (Roche Applied Sciences, Mannheim, Germany) diluted 1:10 in FBS-free cell culture medium. Absorbance was measured at 450 nm and 630 nm (reference wavelength) in a microplate reader. Data was expressed in percentage of the negative control response.

3.   Results and discussion

3.1.   *Corrosion testing*

3.1.1.   *Potentiodynamic polarization*

(i) Influence of medium composition

Fig. 1 presents the polarization curves obtained for the two alloys under study, in the three selected media. The intention of using polarization experiments is not to obtain realistic corrosion rates. For that purpose, mass loss and hydrogen evolution would aid on the estimation of reliable corrosion rates [1,2]. Herein, the aim is to compare how corrosion changes from a mechanistic perspective (i) in different media and (ii) for different alloys.

Mg1Ca alloy. Analyzing the curves in the simplest media (NaCl), it is clear that the behavior of the anodic branch contrasts with curves typically obtained for pure Mg in NaCl, whereby low anodic Tafel slopes synonymous of non-polarizable systems, are obtained [34]. In the present case, the polarization curves obtained for Mg1Ca (Fig. 1, left) show that, in all the three media, there is (i) a difference in the corrosion potential following the order E_{corr} (PBS)< E_{corr} (MEM) < E_{corr} (NaCl) (see Table 3), (ii) a partially protective layer is
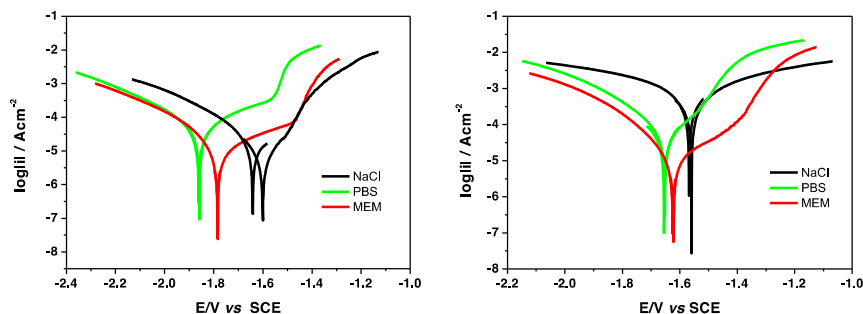

Fig. 1 — **Mg1Ca (left) and Mg10Gd (right) potentiodynamic polarization curves for different electrolyte solutions (0.05 M NaCl, 10 mM PBS and MEM).**

Table 3 – Corrosion potential (E_{corr}), breakdown potential (E_b) and corrosion current density (i_{corr}) for the two biodegradable Mg alloys in the different electrolytes. Weight loss of Mg1Ca and Mg10Gd (for 2 and 7 days immersion) in the different electrolytes are also presented for comparison.

System	Medium	E_{corr}/V	E_b/V	i_{corr}/$\mu A\ cm^{-2}$ (cath branch)	Tafel slope β_c (V)	Weight loss (mg/cm^2) 48 h	SD	Weight loss (mg/cm^2) 168 h	SD
Mg1Ca	NaCl	−1.64	−1.50	25.1	−0.28	7.88	4.08	8.40	1.22
	PBS	−1.86	−1.56	56.2	−0.29	6.95	3.51	46.8	11.8
	MEM	−1.78	−1.46	31.6	−0.30	7.84	2.67	16.8	8.57
Mg10Gd	NaCl	−1.57	−	−	−	184	44.4	252	30.6
	PBS	−1.65	−1.52	178.0	−0.25	140	51.2	248	13.8
	MEM	−1.63	−1.38	39.8	−0.23	12.4	6.90	190	95.4

formed, with different stability ranges, in all the tested media and (iii) the cathodic slopes are similar, although with significantly lower cathodic currents for MEM and PBS. The differences in the E_{corr} cannot be attributed to ohmic drop arising from different conductivity between media, implying that changes in the kinetics of reaction occur with changes in media composition, as shown in previous works available in the literature [35].

In what concerns the stability of the protective layer, formed on the surface in contact with different electrolytes, it is clear that the breakdown potential occurs at more negative potentials in PBS compared to NaCl and MEM, which highlights the relevance of media composition for the buildup of the protective layer, in addition to Cl$^-$, Mg^{2+}, Ca^{2+} and hydroxyl ions, phosphates but also other components previously reported in the literature such as, carbonates [24]. Regarding, corrosion current densities, a rough estimation obtained from the cathodic curves points to Mg1Ca in PBS as the most active system, followed by immersion in NaCl and MEM (Table 3).

Notwithstanding the limitations associated with polarization curves to estimate the corrosion rate of Mg alloys, additional mass loss experiments were performed and the results obtained after 2 and 7 days of immersion are presented in Table 3. These results show that the largest mass loss was found in PBS followed by MEM and NaCl, though the differences between MEM and NaCl are not statistically relevant. Overall, mass loss measurements show the same trend as the one obtained from the polarization curves. Reports in the literature, for weight loss measurements, for Mg1Ca in the media under study, to the best of our knowledge, are not available. There are however, studies for Mg1Ca in an immersion media (HBSS) similar to one of the studied media (PBS) and the results are not far from that obtained in the present work (8.30 mg/cm^2 in HBSS [35] and 6.95 mg/cm^2). The slightly lower value obtained may be due to the fact that immersion time was 48 h whilst the value reported in the literature was for 72 h.

Mg10Gd alloy. Mg10Gd alloy, however, reveals a totally different behavior in NaCl when compared to Mg1Ca: higher currents are measured, even at low overpotentials. This means on one hand that Ca is an important element to render stability to the corrosion product layer formed whereas contrastingly, the possibility of formation of Gd hydrides [36] in Mg10Gd can trigger a more active behavior of this alloy in solution. Additionally, an alloy with such high amount of Gd may have higher tendency towards microgalvanic corrosion. In PBS and MEM, lower current

densities are obtained for low anodic overpotentials and a breakdown potential, missing in NaCl, is now detected in PBS and MEM (Table 3). The E_{corr} values follow the trend observed for Mg1Ca, E_{corr} (PBS)< E_{corr} (MEM)< E_{corr} (NaCl).

In what concerns corrosion current density, this parameter was not estimated for NaCl as the response is fully dominated by the IR drop in this system. The approximate current densities estimated using the cathodic curves in PBS and MEM are presented in Table 3.

With respect to mass loss measurements, the results obtained clearly show the high reactivity of Mg10Gd in NaCl and PBS. In these cases, Mg10Gd specimens were found to fully dissolve after 7 days of immersion, except in MEM, where the mass loss reached was 71.5% of the initial weight (results not shown). Again, the trend observed from the polarization curves for Mg10Gd was confirmed by the mass loss experiments. In the available literature, weight loss measurement data, for Mg10Gd alloy in the media studied, were not found, with the exception of one report for Mg10Gd in 1% of NaCl (immersion time not specified) [35]. The values for weight loss reported (0.54 mg/cm^2) are, however, significantly different from the ones obtained in this work (184 mg/cm^2). This difference may be related to the fact that the immersion period is not specified, wheras our values correspond to a 48 h time frame.

It is noteworthy, that electrochemical measurements assess the corrosion rate in a specific moment of time and can greatly differ from an average corrosion rate during 24 or 168 h, since the kinetics is not linear and the corrosion rate during these periods can significantly change. This fact is also clear when we compare the weight loss of the different systems after different periods (recall Table 3).

(ii) Mg1Ca vs. Mg10Gd

The presence of Ca, in Mg1Ca, may provide additional stability to the corrosion product layer formed even in the simplest NaCl medium while Gd can lead to the formation of hydrides which make Mg10Gd quite active. In spite of observing a partial protective effect of the corrosion products, formed under anodic polarization, Mg1Ca in PBS was found to be the least resistant. This can be due to a combination of different factors namely the increase in concentration of chlorides, approximately 3 times higher when compared to the NaCl solution, and a pH buffering effect, in PBS, that can jeopardize the formation of a more compact layer to protect the alloy more effectively.
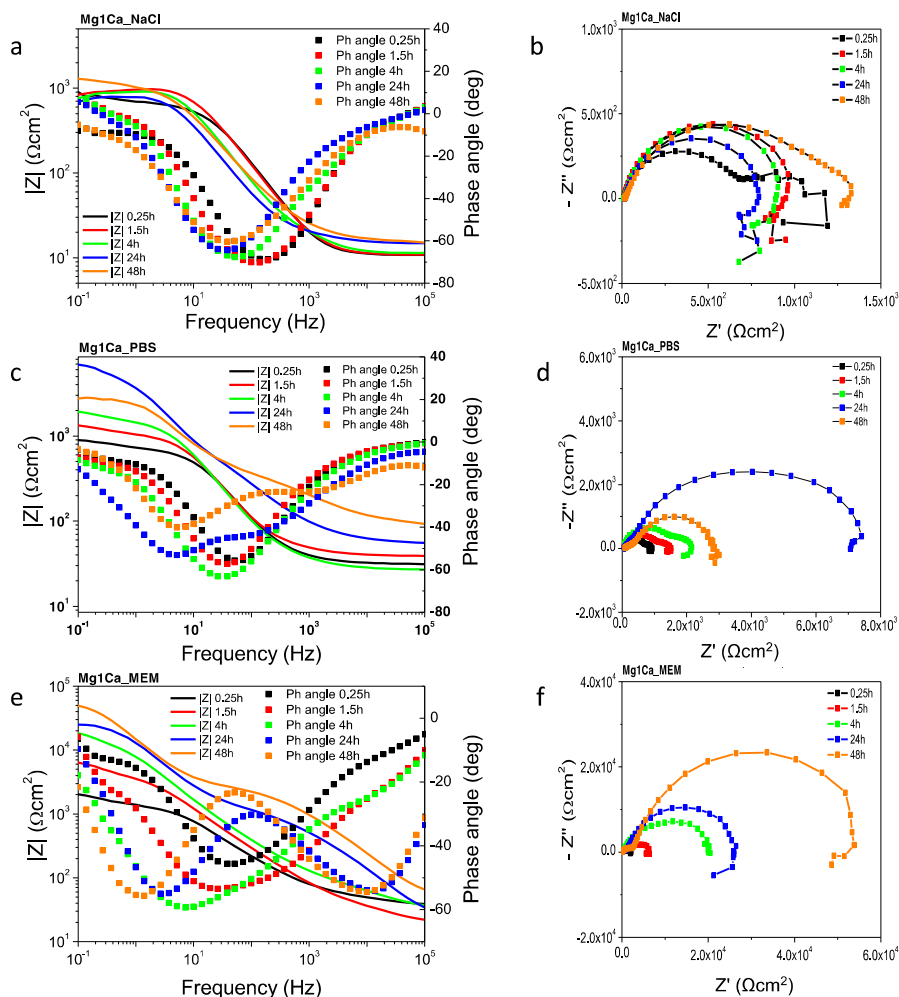
Fig. 2 – EIS spectra acquired for Mg1Ca in different electrolyte solutions (NaCl, PBS and MEM) from 15 min to 48 h of immersion.

These findings are in stark contrast with Mg10Gd, which is most active in NaCl. The presence of additional ingredients in solution such as phosphates provides already some level of protection when compared to the very active Mg10Gd in NaCl, which is considerably more effective in the presence of additional components such as Ca^{2+} and carbonates and fully agrees with previous works [22,24].

3.1.2. EIS studies

Fig. 2a presents EIS spectra acquired for Mg1Ca in 0.05 M NaCl during 48 h of immersion. Two major points can be highlighted from these results: first is that there are no significant changes in the impedance magnitude response over time and the second is the scattering of low frequency points. Going deeper into the analysis of the EIS data, in this frequency region, the fractional residual errors obtained by application of Kramers–Kronig equations increase significantly, up to 24 h, depending upon immersion time. For 48 h of immersion, the number of points with large differences occurs for a smaller frequency range (Fig. 2b). The main reason for this is that after 48 h of immersion the system attains a certain degree of stability in comparison to the initial EIS measurements, thus the

Kramers–Kronig fitting discards a smaller region of spectra affected by the non-stationarity. This is possibly related with the formation of a partial protective layer composed by corrosion products (see EIS detailed discussion below and section 3.2).The OCP values measured before the EIS data acquisition starts at −1.72 V vs. SCE after 15 min of immersion ending up in −1.66 V vs. SCE after two days of immersion (Supplementary Table S1). In the case of Mg1Ca immersed in PBS (Figs 2c and d), the scattering of data is also visible throughout the monitored time. Moreover, the OCP values are initially more negative than in NaCl solution (−1.84 V vs. SCE), tending to increase, with immersion time, up to −1.61 V vs. SCE. Similar to the data acquired in NaCl, the low frequency data cannot be used to evaluate and compare the different systems. In MEM, the OCP values are initially the most negative amidst the different media (−1.86 V vs. SCE), becoming more positive up to 48 h of immersion (−1.58 V vs. SCE). Furthermore, in MEM and PBS, a smaller number of data had to be rejected in comparison to NaCl (Figs 2e and f).

The EIS spectra for Mg10Gd are depicted in Fig. 3. Similarly, several points had to be excluded from the EIS spectra of Mg10Gd alloy based on Kramers–Kronig relations
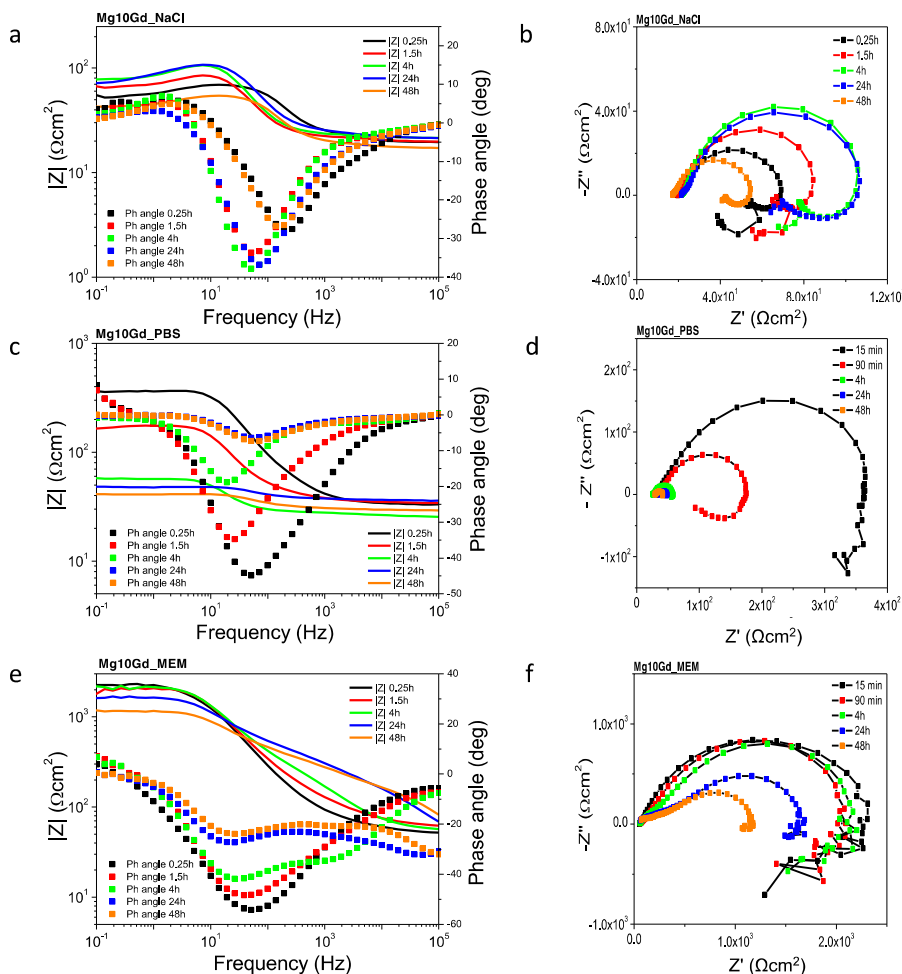
Fig. 3 − EIS spectra acquired for Mg10Gd in different electrolyte solutions (NaCl, PBS and MEM) from 15 min to 48 h of immersion.
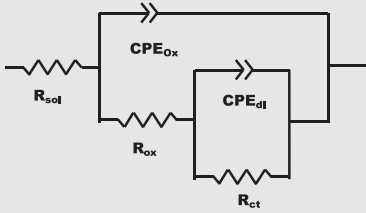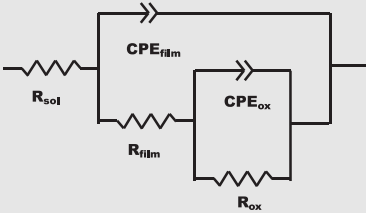
(Supplementary Table S2). Concerning the OCP values, these were quite stable throughout the immersion time being more positive for MEM (−1.52 V vs. SCE), followed by PBS (between −1.61 V and −1.57 V vs. SCE) and NaCl (between −1.66 V and −1.63 V vs. SCE). The OCP values estimated here do not follow, exactly, the order obtained for E_{corr} in the polarization tests (recall Table 3) but are still close to each other (~100 mV). Another important aspect to be mentioned is that for Mg10Gd, in NaCl, the OCP can differ almost 200 mV between replicates (not shown), whereas for the other media this difference is smaller than 80 mV (PBS) and 40 mV (MEM).

The reason behind the description of the Kramers−Kronig analysis in detail, in this work, is to show that one cannot use low frequency data to extract any information concerning inductive behavior of these Mg alloys and, therefore, estimate polarization resistance and corrosion rate according to the procedure described by King et al. [37]. As a result, the fitting of EIS data described below was done after excluding the low frequency data which did not comply with Kramers−Kronig analysis.

The EIS data were fitted using the equivalent circuits presented in Table 4 and are based on studies recently presented in the literature [38,39]. In the beginning in NaCl, one time constant at intermediate frequencies could be detected. One additional time constant could be observed at low frequencies, although the number of points available were not enough to fit and obtain meaningful values. The first time constant presents an order of magnitude typically associated with a thin layer of oxides, represented by a constant-phase element (CPE_{ox}) in parallel with an oxide resistor (R_{ox}). The low frequency time constant is ascribed to the ongoing electrochemical (corrosion processes), represented by a constant phase element (CPE_{dl}) in parallel with a charge transfer resistor (R_{ct}). Moreover, with evolution of immersion time, the same time constants were observed but there was an increase in the R_{ox} (from 5.48×10^2 to 1.24×10^3 Ω cm^2).

Fig. 4 depicts the resistance of the oxide layer protecting the substrate (R_{ox}). In PBS solution, the EC used to fit the EIS is the same used to adjust the EIS data in NaCl. Initially, only the time constant at intermediate frequencies, mainly

Table 4 − EC circuits used to fit EIS impedance for Mg1Ca and Mg10Gd in different media (Constant-phase elements were used instead of pure capacitors).

Equivalent circuit	Alloy	
	Mg1Ca	Mg10Gd
(circuit with R_{sol}, CPE_{ox}, R_{ox}, CPE_{dl}, R_{ct})	NaCl (0−48 h) PBS (0−24 h) MEM (0−4 h)	NaCl (0−48 h) PBS (0−48 h) MEM (0−1.5 h)
(circuit with R_{sol}, CPE_{film}, R_{film}, CPE_{ox}, R_{ox})	PBS (48 h) MEM (24−48 h)	MEM (4−48 h)

associated with the oxide film, could be fitted, although the corrosion process is also present. However, as the time evolves, the system becomes more protected and, for long immersion times (48 h), a high frequency time constant appears, which can be correlated with the growth of an additional protective film (CPE_{film} in parallel with R_{film}), thus the system can now be represented by a two time constant associated with a protective layer and a more internal oxide layer (Table 4).

In MEM, two time constants were initially detected, similarly to the results obtained in NaCl and PBS. The time constant at intermediate frequencies is ascribed to the oxide, while the time constant at low frequencies is associated with corrosion processes. Nevertheless, the latter could not be fitted as there were not sufficient data after exclusion of points based on Kramers−Kronig relations. With evolution of immersion time a high frequency time-constant appears after 24 h. The effective capacitance (not shown) is almost two orders of magnitude lower and seems to be consistent with the

growth of an additional protective layer for longer immersion times. Nevertheless, the substrate is more protected in MEM when compared to PBS, with R_{ox} being 20 times higher in MEM than in PBS after 48 h of immersion (Fig. 4 a).

Looking into the Bode and Nyquist representation of EIS spectra for Mg10Gd (Fig. 3), after 15 min of immersion in NaCl, one time constant at intermediate frequencies could be detected. Although the effective capacitance suggests that it can be related with the oxide layer grown in contact with the solution, the R_{ox} obtained, using the EC presented in Table 4, is more than one order of magnitude lower when compared to Mg1Ca, varying between 3.92×10^1 to 1.20×10^2 Ω cm^2 (Fig. 4 b). In PBS, the reactivity of Mg10Gd is even more remarkable: only the intermediate time constant can be fitted. However, there is a remarkable decrease in the impedance between 1.5 h and 4 h. This decrease in impedance corresponds to an increase of almost four times (from 94 to 347 μF cm^{-2}) in the effective capacitance of the fitted time constant. Such difference can be explained in the following way: for short immersion times
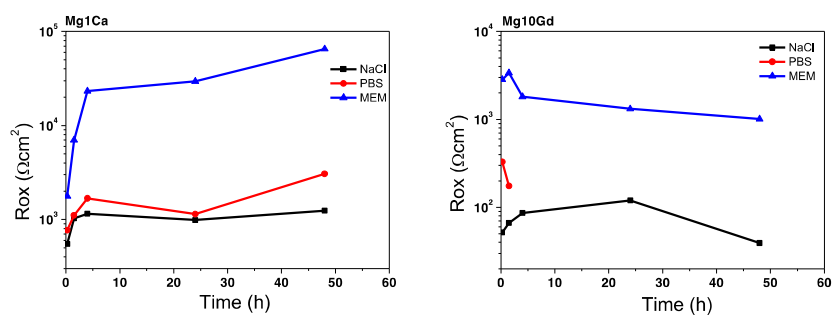

Fig. 4 − Evolution of (R_{ox}) as a function of time for Mg1Ca and Mg10Gd(*) in different media (*) for the system Mg10Gd in PBS only Rox values up to 4 h of immersion were determined. For longer immersion periods Rox values could not be fitted due to the a high degree of uncertainty associated with those.

there is an effect of the buildup of corrosion products in PBS, but as time evolves, its protective abilities are no longer verified and the response of the system is dominated by the ongoing corrosion processes. As a result, up to 4 h of immersion the time constant fitted corresponds to the response of the oxide layer, whereas for longer immersion times it corresponds to the double layer response and ongoing electrochemical processes. In the case of Mg10Gd immersed in MEM, the results are qualitatively similar to the ones obtained for Mg1Ca: for short immersion times (t < 4 h) the intermediate time constant is associated with the response of the corrosion product layer, whereas after 4 h of immersion an additional time constant associated with the growth of a film is observed and consistent with results previously reported for metals immersed in Ca-containing electrolytes [24].

In line with the analysis presented above, it is possible to observe that Mg1Ca has a lower degradation, in all the tested media when compared to Mg10Gd. Moreover, both alloys are more protected in MEM when compared to PBS and NaCl solution. These results are quite relevant: MEM has all the ingredients to build up a protective layer which drastically reduces the corrosion of Mg alloys, even when the alloy is active. One remark concerning the comparison of EIS results with mass loss measurements presented in Table 3 should be considered at this point. The results from EIS are in agreement with mass loss measurements, except for Mg1Ca in NaCl and MEM. The mass loss measurements do not show statistical differences in the corrosion rate of Mg1Ca in MEM and NaCl. In fact, the mean value of weight loss is larger in MEM than in NaCl. This may be due to the buildup of the protective layer in MEM which is thicker, but also grows at the expense of some dissolution of Mg from the underlying substrate.

Thus, not only is MEM providing an active corrosion protection to the studied Mg alloys but is also a relevant medium for *in vitro* cell growth and toxicity testing. Furthermore, MEM closely mimics *in vivo* environment. Though its levels of Ca and Mg are slightly lower compared with blood, it contains glucose, amino acids, and vitamins, and similar concentration of HPO_4^{2-} and HCO_3^-. As a result, MEM should be selected to probe the degradation of Mg alloys under more realistic conditions [40].

3.2. Structural, compositional and morphological characterization

Fig. 5 presents the surface morphologies and corresponding EDS spectra for both Mg alloys, before and after 48 h immersion, in different electrolytes. Before immersion, SEM
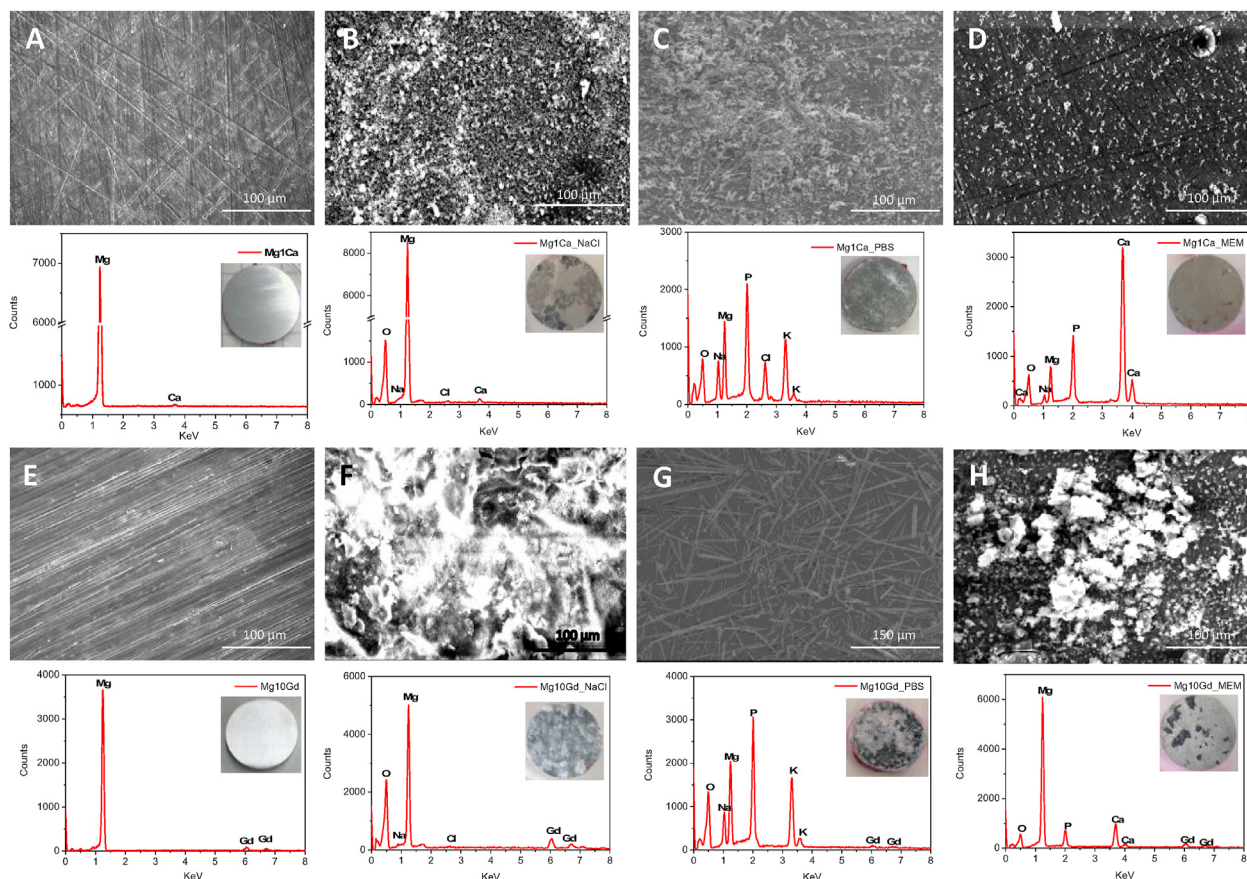

Fig. 5 — SEM images and corresponding EDS spectra of Mg1Ca and Mg10Gd alloys before and after 48 h immersion in different electrolytes. Mg1Ca (A) as-polished, after 48 h immersion in (B) NaCl (C) PBS immersion and (D) MEM. Mg10Gd (E) as-polished, after 48 h immersion in (F) NaCl (G) PBS and (H) MEM.
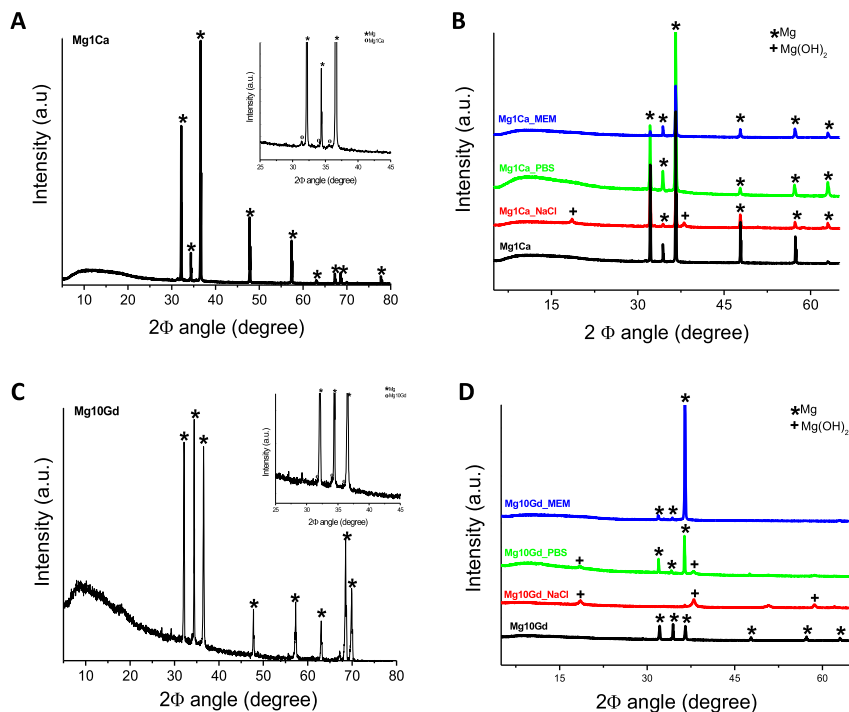
Fig. 6 − A: XRD spectra of polished Mg1Ca alloy (inset showing Mg1Ca phases); B XRD spectra of Mg1Ca alloy after 48 h immersion in different media. C: XRD spectrum of polished Mg10Gd alloy (inset showing Mg10Gd phases); D: XRD spectra of Mg10gd alloy after 48 h immersion in different media.

images of the surface of Mg1Ca (panel A) and Mg10Gd (panel E) substrates reveal micro scratches arising from the polishing procedure used to remove oxides from the surface, whilst EDS spectra show the main constituents of the alloys: Mg and Ca for Mg1Ca and Mg and Gd for Mg10Gd. The optical images presented as insets in the EDS spectra show substrates with clean, shiny surfaces. After 48 h of immersion in the different media, two main points can be highlighted: (i) Mg1Ca substrates (panels B, C and D) show less corrosion products than Mg10Gd for the same media (panels F, G and H) and (ii) both alloys show less corrosion products when tested in MEM, which is in agreement with the previous electrochemical measurements.

Moreover, the high corrosion activity identified earlier for Mg10Gd in NaCl can be directly associated with the extensive amount of corrosion products deposited on the surface (panel F). Regarding the compositional analysis by EDS, the analysis of the deposits, after immersion in NaCl, shows the presence of signals associated with O, Na and Cl, which is consistent with the formation of hydroxides and oxides of Mg and contamination of the surface with NaCl salts. The corrosion products in this case show a grainy-like morphology.

In PBS, a strong signal of P and K allows us to infer the incorporation of these elements in the layer of deposits formed on the substrate. In addition, the morphology of the deposits formed is different: for Mg1Ca there is the formation of needles and particle-like products, while for Mg10Gd only needles are observed. In MEM, Mg10Gd shows more compact

products (panel H) with Ca incorporated, which may explain why the corrosion of this alloy is lower in MEM than in other media, although the high signal of Mg detected together with O, may indicate the formation of Mg corrosion products to some extent. In the case of Mg1Ca, the product layer formed is thin enough to detect the scribes from the polishing procedure initially carried out, with the signal of Ca and P prevailing in the associated EDS spectrum (panel D). Overall, all the obtained results are consistent with the electrochemical findings previously presented.

The XRD patterns acquired from the samples exposed to the different electrolytes, for 48 h, are shown in Fig. 6. Panels A and C show the main diffraction peaks associated with the bare substrates [41−43] and panels B and D show the overlapping of XRD diffractograms for Mg1Ca (B) and Mg10Gd (D) after exposure in different media.

Mg1Ca and Mg10Gd bare substrates present peaks at 2Φ angles around 32°, 34°, 36°, 47°, 57°, 63°, 69° and 70° corresponding to (100) (002) (101) (102) (110) (103) (112) and (201) crystal planes of Mg respectively (JCPDS card number 04-007-3847). Mg1Ca also present a reflection from (202) crystal plane of Mg at 2Φ angle around 78°.

In the case of Mg1Ca, after exposure to different media (Fig. 6B), all the substrates present peaks mainly associated with Mg substrate. Only in NaCl the reflection planes at 2Φ angle around 18°, and 38° related with (001) and (011) crystal planes indexed to Mg(OH)$_2$ phases were detected (JCPDS card number 04-015-4256). In PBS and MEM only peaks of Mg alloys were

observed. This implies that the deposits formed and observed before (Fig. 5) are too thin (and possibly amorphous) to be detected by XRD.

For Mg10Gd, corrosion activity was significant in NaCl medium and for that reason a thick porous layer of corrosion products was detected. Hence, only the signal of $Mg(OH)_2$ was observed, revealed by the presence of 2Φ angles around 18°, 38°, 51° and 58° corresponding to (001) (011) (102) and (110) crystal planes of $Mg(OH)_2$ phases respectively (JCPDS card number 04-016-3445). In PBS the corrosion was not as extensive and signal from the Mg substrate is still detected (2Φ angles around 32°, 34° and 36° related to 100, 002 and 101 Mg phases), in addition to (001) and (101) crystal planes associated with $Mg(OH)_2$ phases at 2Φ angles around 18° and 38° (JCPDS card number 04-015-2580 and 01-075-1527). Finally, in MEM

only diffraction peaks associated with Mg can be detected. Again, these findings support the amorphous nature of the protective layer formed in MEM, which is in full agreement with previous work by Mei [24].

3.3. Cytotoxicity testing

Cells were exposed to the Mg1Ca and Mg10Gd extracts for 24 h and cytotoxicity was evaluated using two well-established endpoints: LDH release, an indicator of plasma membrane integrity and WST-1 reduction to assess changes in cell metabolic activity. The appearance of the Mg1Ca and Mg10Gd alloys and respective extracts after the 24- and 72-h extraction is pictured in Fig. 7. The degradation behavior of the bare Mg alloys, especially of Mg10Gd was rather inhomogeneous among the extraction experiments as evidenced by variance of the data. Regarding the cytotoxicity of the Mg1Ca, neither the direct nor the diluted 24-h extracts caused significant alterations in cell viability compared to the respective controls, as assessed by the LDH release and WST-1 reduction assays (Fig. 8A and B). Our findings are in agreement with previous studies reporting the absence of significant *in vitro* cytotoxicity following indirect exposure to Ca-alloyed Mg alloys [44–46]. However, the 72-h Mg1Ca extracts induced a concentration-dependent increase of LDH release in L929-exposed cells (Fig. 8C) and a significant decrease in cellular metabolic activity ($62 \pm 15\%$ of negative control) in cells incubated 24 h with the direct extract (Fig. 8D). Indeed, a higher degree of Mg1Ca alloy dissolution was observed at 72 h compared to 24 h after extraction. Mg levels in the direct extracts increased comparing with the extraction medium, being this increase more evident in the 72-h extracts (7.29 ± 0.18 *vs* 0.79 ± 0.002 mM). At the same time, Ca concentration in the extract decreased at 72 h (0.47 ± 0.05 *vs* 1.55 ± 0.15 mM), probably caused by Ca precipitation due to medium alkalization. Accordingly, cytotoxicity at this timepoint is most likely caused by elevation of the Mg content, H_2 gas evolution and pH alkalization as previously reported for Mg alloys [47–49].

On the other hand, a significant concentration-dependent increase, in LDH release, was observed in cells exposed to the 24-h Mg10Gd extracts when compared to the corresponding controls (Fig. 8A). This was accompanied by a significant decrease of WST-1 reduction observed in L929 cells exposed to direct Mg10Gd alloy extract (Fig. 8B). Moreover, Mg10Gd 72-h extracts induced a marked cytotoxicity in L929 cells. The cell metabolic activity was significantly reduced ($6 \pm 0.1\%$ of NC) in L929 cells incubated with the direct extract compared with the corresponding control (Fig. 8D). However, LDH release levels in the very same cells were close to zero (Fig. 8C), suggesting an interference of the extract in the assay. Indeed, pH measurements of the extracts revealed a pH 12 value for the Mg10Gd extracts contrasting with the pH 8.5 value observed in the FBS-free cell culture medium kept under the same extraction conditions. This rise in pH could explain the changes in cell viability detected. To test this hypothesis, Mg10Gd extract pH was adjusted to 8.5 and tested for cytotoxicity. As shown in Fig. 9, a significant increase of LDH release ($71 \pm 8\%$ of PC) was now detected in cells exposed to the pH-adjusted Mg10Gd extract. On the other hand, a marked decrease in cell metabolic activity ($20 \pm 5\%$ of NC) consistent with the effect caused by exposure to
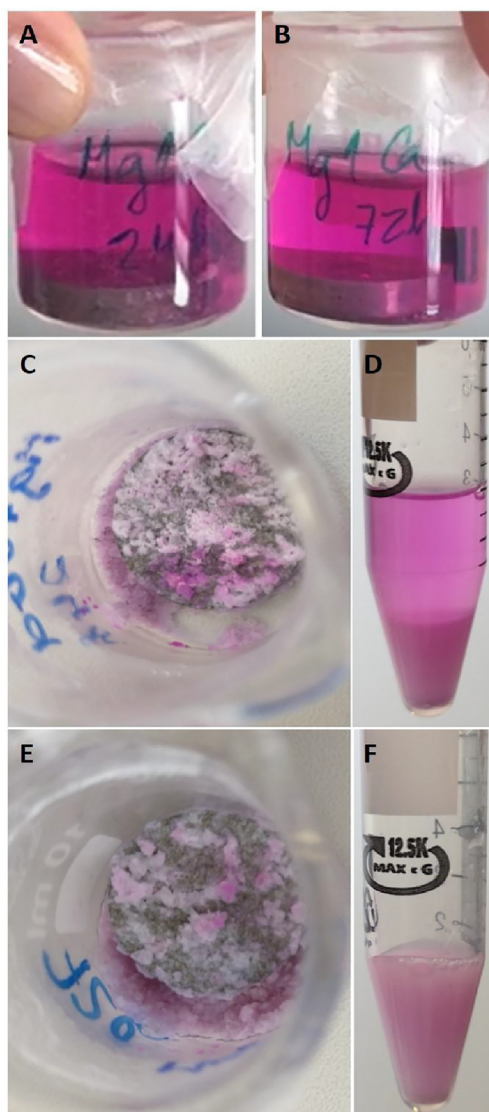

Fig. 7 – Pictures of the Mg alloys and extracts after the 24-h and 72-h extraction in serum-free cell culture medium. Mg1Ca alloys and extract after 24 h (A); Mg1Ca alloys and extract after 72 h of incubation (B); Mg10Gd alloy and extract after 24 h (C and D, respectively); Mg10Gd alloy and extract after 72 h (E and F, respectively).
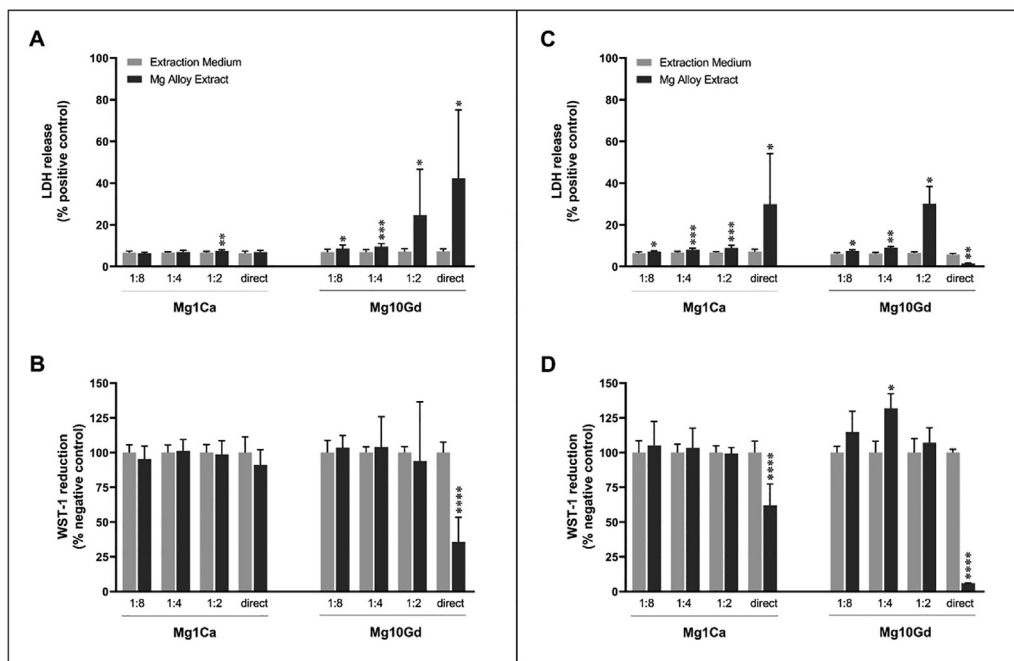
Fig. 8 – Effect of the Mg alloys extracts on L929 cells viability. Left (A) Plasma membrane integrity (LDH release) and (B) cell metabolic activity (WST-1 reduction) after 24 h exposure to the 24-h extracts. Right (C) Plasma membrane integrity (LDH release) and (D) cell metabolic activity (WST-1 reduction) after 24 h exposure to the 72-h extracts. Data represent the mean ± standard deviation (SD) of three independent experiments, each performed in triplicate. Data was analyzed using Welch's t test. *p < 0.05, **p < 0.01, ***p < 0.001; ****p < 0.0001 vs extraction medium.

the Mg10Gd 72-h extract was observed showing that, despite interfering with the LDH release measurements, this extract is highly cytotoxic, most likely due to its Gd content. In this regard, Grillo et al. investigated *in vitro* cytotoxicity of Gd, either alone or in mixtures with Mg ions, in Chinese hamster ovary (CHO−K1) cells. These authors showed cytotoxic effects at Gd concentration levels ≥200 μM, though no synergistic effects were observed for Gd−Mg mixtures. On the other hand, Kottuparambil et al. reported no significant adverse effects on mouse embryo fibroblast NIH 3T3 cells cultured onto Gd-alloyed Mg alloy disks (Mg-Zn-Gd and Mg−Zn-Gd-Nd) [50]. In our study, Gd concentrations in the direct extracts are around 0.4 μM. However, other elements such as Al (0.5 μM), Zn (0.2 μM), Cu (0.4 μM) and Sr (0.2 μM)

were also detected in Mg10Gd extracts and may contribute additively and/or synergistically to the observed cytotoxic effects. Gd toxicity in humans is still a matter of spark debate mostly from the evidence of Gd accumulation and reports of harmful effects in patients subjected to magnetic resonance imaging (MRI) using Gd-based contrast agents [45]. Furthermore, Mg−Gd alloys seem to be rapidly degraded *in vivo*. Myrissa et al. reported that Mg10Gd pins implanted into Sprague−Dawley rats were fragmented just 12 weeks after implantation to smaller particles that perturbed bone remodeling. The released Gd distributed and accumulated in various organs, mainly in the spleen, lung, liver and kidney over the 36 weeks of study [51,52].
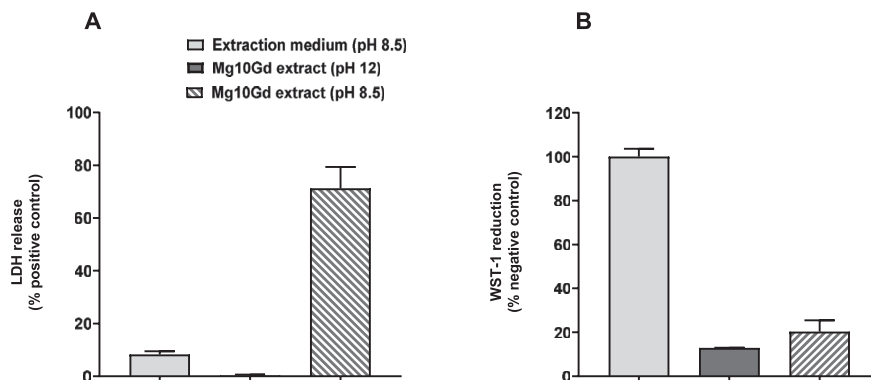

Fig. 9 – Effect of the Mg10Gd alloy 24-h extract, as extracted (pH 12) and after pH adjustment (pH 8.5) in L929 cells viability (A) Plasma membrane integrity (LDH release) and (B) cell metabolic activity (WST-1 reduction) following 24 h of exposure. Data represent the mean ± standard deviation (SD) of one experiment performed in triplicate.

Thus, more studies must be performed to investigate the safety of Gd-alloyed Mg alloys.

4.   Conclusions

In this work, two biodegradable Mg alloys were tested in different media to evaluate their corrosion degradation and induced cytotoxicity. The main conclusions obtained are as follows:

- The electrochemical results showed that Mg1Ca has a lower degradation rate when compared to Mg10Gd, due to the presence of Ca as an alloying element.
- The corrosion activity was reduced in MEM, for both alloys, when compared to NaCl and PBS. These results are in line with previous works reported in the literature.
- The results obtained with electrochemical techniques are consistent with mass loss measurements performed for both alloys in different media.
- Although MEM is a more complex medium for unveiling mechanistic information, regarding the degradation of Mg alloys, it gives additional protection and thus more realistic results when the purpose of the work is the development of materials for biomedical applications.
- Concerning cytotoxicity studies, Mg10Gd was found to be cytotoxic in all the conditions tested, while the toxicity of Mg1Ca was low.
- For high extract concentrations some toxicity was also found for Mg1Ca, meaning that additional control on the dissolution of the alloy should be considered.

Declaration of Competing Interest

The authors declare that they have no known competing financial interests or personal relationships that could have appeared to influence the work reported in this paper.

Acknowledgements

Appendix A. Supplementary data

Supplementary data to this article can be found online at https://doi.org/10.1016/j.jmrt.2021.05.090.

REFERENCES

[1] Staiger MP, Pietak AM, Huadmai J, Dias G. Magnesium and its alloys as orthopedic biomaterials: a review. Biomaterials 2006;27:1728—34.

[2] Yang JX, Cui FZ, Lee IS. Surface modifications of magnesium alloys for biomedical applications. Ann Biomed Eng 2011;39:1857—71.

[3] Rosalbino F, De Negri S, Saccone A, Angelini E, Delfino S. Bio-corrosion characterization of Mg-Zn-X (X = Ca, Mn, Si) alloys for biomedical applications. J Mater Sci Mater Med 2010;21:1091—8.

[4] Hornberger H, Virtanen S, Boccaccini AR. Biomedical coatings on magnesium alloys - a review. Acta Biomater 2012;8:2442—55.

[5] Esmaily M, Svensson JE, Fajardo S, Birbilis N, Frankel GS, Virtanen S, et al. Fundamentals and advances in magnesium alloy corrosion. Prog Mater Sci 2017;89:92—193.

[6] Zheng YF, Gu XN, Witte F. Biodegradable metals. Mater Sci Eng R Rep 2014;77:1—34.

[7] Yang Y, He C, E D, Yang W, Qi F, Shen L, et al. Mg bone implant: features, developments and perspectives. Mater Des 2020;185:108259.

[8] Navarro M, Michiardi A, Castano O, Planell JA. Biomaterials in orthopaedics. J R Soc Interface 2008;5:1137—58.

[9] Song GL, Atrens A. Corrosion mechanisms of magnesium alloys. Adv Eng Mater 1999;1:11—33.

[10] Song G, Atrens A. Understandings magnesium corrosion. Adv Eng Mater 2003;5:837—56.

[11] Zeng RC, Yin ZZ, Chen XB, Xu DK. Corrosion types of magnesium alloys. In: Tanski T, Borek W, Król M, editors. Magnesium alloys - selected issue. Intech Open; 2018.

[12] Witte F, Hort N, Vogt C, Cohen S, Kainer KU, Willumeit R, et al. Degradable biomaterials based on magnesium corrosion. Curr Opin Solid State Mater Sci 2008;12:63—72.

[13] Guan S, Hu J, Wang L, Zhu S, Wang H, Wang J, et al. Mg alloys development and surface modification for biomedical application. In: Czerwinski F, editor. Magnesium alloys - corrosion and surface treatments. InTech; 2011.

[14] Chen YJ, Xu ZG, Smith C, Sankar J. Recent advances on the development of magnesium alloys for biodegradable implants. Acta Biomater 2014;10:4561—73.

[15] Yang QY, Yuan W, Liu XM, Zheng YF, Cui ZD, Yang XJ, et al. Atomic layer deposited ZrO2 nanofilm on Mg-Sr alloy for enhanced corrosion resistance and biocompatibility. Acta Biomater 2017;58:515—26.

[16] Chen XB, Nisbet DR, Li RW, Smith PN, Abbott TB, Easton MA, et al. Controlling initial biodegradation of magnesium by a biocompatible strontium phosphate conversion coating. Acta Biomater 2014;10:1463—74.

[17] Yao ZP, Xia QX, Chang LM, Li CN, Jiang ZH. Structure and properties of compound coatings on Mg alloys by micro-arc oxidation/hydrothermal treatment. J Alloys Compd 2015;633:435—42.

[18] Scharnagl N, Blawert C. 14 - polymer-based degradable coatings for metallic biomaterials. In: Wen C, editor. Surface coating and modification of metallic biomaterials. Woodhead Publishing; 2015. p. 393—422.

[19] Gu XN, Zheng YF, Chen LJ. Influence of artificial biological fluid composition on the biocorrosion of potential orthopedic Mg-Ca, AZ31, AZ91 alloys. Biomed Mater 2009;4:065011.

[20] Xin Y, Chu PK. Influence of Tris in simulated body fluid on degradation behavior of pure Magnesium. Mater Chem Phys 2010;124:33—5.

[21] Xin Y, Hu T, Chu PK. Influence of test solutions on in vitro studies of biomedical magnesium alloys. J Electrochem Soc 2010;157:C238—43.

[22] Agha NA, Feyerabend F, Mihailova B, Heidrich S, Bismayer U, Willumeit-Romer R. Magnesium degradation influenced by buffering salts in concentrations typical of in vitro and in vivo models. Mater Sci Eng C Mater Biol Appl 2016;58:817—25.

[23] Yamamoto A, Hiromoto S. Effect of inorganic salts, amino acids and proteins on the degradation of pure magnesium in vitro. Mater Sci Eng C 2009;29:1559—68.

[24] Mei D, Lamaka SV, Gonzalez J, Feyerabend F, Willumeit-Romer R, Zheludkevich ML. The role of individual components of simulated body fluid on the corrosion behavior of commercially pure Mg. Corrosion Sci 2019;147:81—93.

[25] Witte F, Kaese V, Haferkamp H, Switzer E, Meyer-Lindenberg A, Wirth CJ, et al. In vivo corrosion of four magnesium alloys and the associated bone response. Biomaterials 2005;26:3557—63.

[26] Witte F, Fischer J, Nellesen J, Crostack HA, Kaese V, Pisch A, et al. In vitro and in vivo corrosion measurements of magnesium alloys. Biomaterials 2006;27:1013—8.

[27] Heublein B, Rohde R, Kaese V, Niemeyer M, Hartung W, Haverich A. Biocorrosion of magnesium alloys: a new principle in cardiovascular implant technology? Heart 2003;89:651—6.

[28] Peeters P, Bosiers M, Verbist J, Deloose K, Heublein B. Preliminary results after application of absorbable metal stents in patients with critical limb ischemia. J Endovasc Ther 2005;12:1—5.

[29] Abd El-Rahman SS. Neuropathology of aluminum toxicity in rats (glutamate and GABA impairment). Pharmacol Res 2003;47:189—94.

[30] Nakamura Y, Tsumura Y, Tonogai Y, Shibata T, Ito Y. Differences in behavior among the chlorides of seven rare earth elements administered intravenously to rats. Fund Appl Toxicol 1997;37:106—16.

[31] Li N, Zheng YF. Novel magnesium alloys developed for biomedical application: a review. J Mater Sci Technol 2013;29:489—502.

[32] Campos MDS, Blawert C, Mendis CL, Mohedano M, Zimmermann T, Proefrock D, et al. Effect of heat treatment on the corrosion behavior of Mg-10Gd alloy in 0.5% NaCl solution. Frontiers in Materials 2020;7.

[33] ISO10993-4, Biological evaluation of medical devices - Part 4: selection of tests for interactions with blood.

[34] Song G, Atrens A, John DS, Wu X, Nairn J. The anodic dissolution of magnesium in chloride and sulphate solutions. Corrosion Sci 1997;39:1981—2004.

[35] Kirkland NT, Birbilis N, Staiger MP. Assessing the corrosion of biodegradable magnesium implants: a critical review of current methodologies and their limitations. Acta Biomater 2012;8:925—36.

[36] Huang Y, Yang L, You S, Gan W, Kainer KU, Hort N. Unexpected formation of hydrides in heavy rare earth containing magnesium alloys. Journal of Magnesium and Alloys 2016;4:173—80.

[37] King AD, Birbilis N, Scully JR. Accurate electrochemical measurement of magnesium corrosion rates; a combined impedance, mass-loss and hydrogen collection study. Electrochim Acta 2014;121:394—406.

[38] Song G-L, Unocic KA. The anodic surface film and hydrogen evolution on Mg. Corrosion Sci 2015;98:758—65.

[39] Deng M, Wang L, Höche D, Lamaka SV, Wang C, Snihirova D, et al. Approaching "stainless magnesium" by Ca micro-alloying. Materials Horizons 2021:589—96.

[40] Pogorielov M, Husak E, Solodivnik A, Zhdanov S. Magnesium-based biodegradable alloys: degradation, application, and alloying elements. Interventional Medicine and Applied Science 2017;9:27—38.

[41] Nowosielski R, Gawlas-Mucha A, Borowski A, G A. Fabrication and properties of magnesium based alloys Mg-Ca. Journal of Achievements in Materials and Manufacturing Engineering 2013:61.

[42] Hort N, Huang Y, Fechner D, Stormer M, Blawert C, Witte F, et al. Magnesium alloys as implant materials–principles of property design for Mg-RE alloys. Acta Biomater 2010;6:1714—25.

[43] Schluter K, Shi ZM, Zamponi C, Cao FY, Quandt E, Atrens A. Corrosion performance and mechanical properties of sputter-deposited MgY and MgGd alloys. Corrosion Sci 2014;78:43—54.

[44] Ding PF, Liu YC, He XH, Liu DB, Ghen MF. In vitro and in vivo biocompatibility of Mg-Zn-Ca alloy operative clip. Bioactive Materials 2019;4:236—44.

[45] Xia YH, Zhang BP, Wang Y, Qian MF, Geng L. In-vitro cytotoxicity and in-vivo biocompatibility of as-extruded Mg-4.0Zn-0.2Ca alloy. Materials Science & Engineering C-Materials for Biological Applications 2012;32:665—9.

[46] Zhang BP, Hou YL, Wang XD, Wang Y, Geng L. Mechanical properties, degradation performance and cytotoxicity of Mg-Zn-Ca biomedical alloys with different compositions. Materials Science & Engineering C-Materials for Biological Applications 2011;31:1667—73.

[47] Wang JL, Qin L, Wang K, Wang J, Yue Y, Li YD, et al. Cytotoxicity studies of AZ31D alloy and the effects of carbon dioxide on its biodegradation behavior in vitro. Materials Science & Engineering C-Materials for Biological Applications 2013;33:4416—26.

[48] Fischer J, Profrock D, Hort N, Willumeit R, Feyerabend F. Reprint of: improved cytotoxicity testing of magnesium materials. Materials Science and Engineering B-Advanced Functional Solid-State Materials 2011;176:1773—7.

[49] Liu XL, Xi TF, Zheng YD. Influence of the extraction parameters on the cytotoxicity test results of Mg materials. Progress in Natural Science-Materials International 2014;24:507—15.

[50] Kottuparambil RR, Bontha S, Rangarasaiah RM, Arya SB, Jana A, Das M, et al. Effect of zinc and rare-earth element addition on mechanical, corrosion, and biological properties of magnesium. J Mater Res 2018;33:3466—78.

[51] Myrissa A, Braeuer S, Martinelli E, Willumeit-Romer R, Goessler W, Weinberg AM. Gadolinium accumulation in organs of Sprague-Dawley (R) rats after implantation of a biodegradable magnesium-gadolinium alloy. Acta Biomater 2017;48:521—9.

[52] Rogosnitzky M, Branch S. Gadolinium-based contrast agent toxicity: a review of known and proposed mechanisms. Biometals 2016;29:365—76.